ACS APPLIED ENERGY MATERIALS

www.acsaem.org Article

Reactive Vapor-Phase Additives toward Destabilizing γ-$Mg(BH_4)_2$ for Improved Hydrogen Release

Nicholas A. Strange, Noemi Leick, Sarah Shulda, Andreas Schneemann, Vitalie Stavila, Andrew S. Lipton, Michael F. Toney, Thomas Gennett, and Steven T. Christensen*

Cite This: *ACS Appl. Energy Mater.* 2022, 5, 1690–1700 Read Online

ACCESS | Metrics & More | Article Recommendations | Supporting Information

ABSTRACT: Magnesium borohydride ($Mg(BH_4)_2$) is a promising candidate for material-based hydrogen storage due to its high hydrogen gravimetric/volumetric capacities and potential for dehydrogenation reversibility. Currently, slow dehydrogenation kinetics and the formation of intermediate polyboranes deter its application in clean energy technologies. In this study, a novel approach for modifying the physicochemical properties of $Mg(BH_4)_2$ is described, which involves the addition of reactive molecules in the vapor phase. This process enables the investigation of a new class of additive molecules for material-based hydrogen storage. The effects of four molecules (BBr_3, $Al_2(CH_3)_6$, $TiCl_4$, and N_2H_4) with varying degrees of electrophilicity are examined to infer how the chemical reactivity can be used to tune the additive−$Mg(BH_4)_2$ interaction and optimize the release of hydrogen at lower temperatures. Control over the amounts of additive exposure to $Mg(BH_4)_2$ is shown to prevent degradation of the bulk γ-$Mg(BH_4)_2$ crystal structure and loss of hydrogen capacity. Trimethylaluminum provides the most encouraging results on $Mg(BH_4)_2$, maintaining 97% of the starting theoretical $Mg(BH_4)_2$ hydrogen content and demonstrating hydrogen release at 115 °C. These results firmly establish the efficacy of this approach toward controlling the properties of $Mg(BH_4)_2$ and provide a new path forward for additive-based modification of hydrogen storage materials.

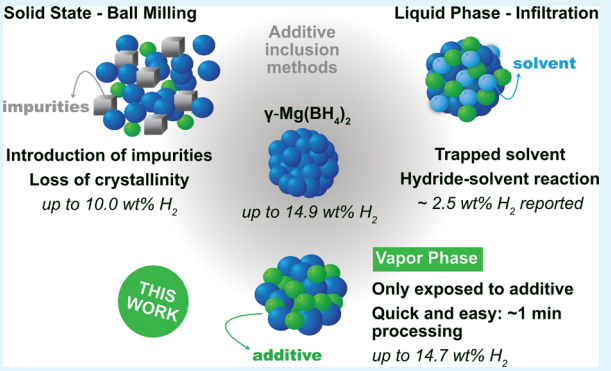

KEYWORDS: *magnesium borohydride, hydrogen storage, electrolytes, additives, vapor-phase chemistry, synchrotron radiation*

INTRODUCTION

Hydrogen has long been considered the quintessential energy carrier due to its unrivaled energy density and absence of carbon emissions. As domestic and international leaders alike begin to adopt new clean energy strategies,[1−4] the demand for "green hydrogen" is expected to increase dramatically over the next few decades. Although hydrogen possesses desirable characteristics as an energy carrier, the development of efficient methods for storage and delivery remains a challenge. Complex hydrides, and in particular borohydrides, represent one class of materials that have demonstrated promise as potential solid-state hydrogen storage media, exhibiting a high gravimetric hydrogen content and relatively low decomposition enthalpies. These compounds also have broad application as reducing agents in synthetic chemistry[5] and more recently have been investigated for their ion conductivities in solid-state batteries.[6] Among various hydrogen storage-based applications, magnesium borohydride ($Mg(BH_4)_2$) is widely regarded as a pre-eminent candidate storage material due to its 14.9 wt % theoretical gravimetric H_2 capacity, 113 g/L volumetric capacity, moderate decomposition temperature (~280 °C),[7] and potential for reversibility. On a materials basis, these physiochemical properties address many of the technical performance targets established by the U.S. Department of Energy for onboard hydrogen storage systems in light-duty vehicles.[8] Despite these favorable properties, ($Mg(BH_4)_2$) suffers from extremely poor decomposition kinetics and the formation of metastable polyborane intermediates and MgB_2, which require high temperatures and pressures for rehydrogenation.

The γ-phase of $Mg(BH_4)_2$ was originally advertised for its high internal surface area (~1150 m^2/g) and potential for hybridized chemical/physical storage capabilities having ~30% void space.[9] It was theorized that the higher surface-to-volume ratio would enable faster solid-state proton diffusion to the surface and improve dehydrogenation kinetics as suggested by the enhanced rates of proton-deuterium exchange measure-

Received: October 6, 2021
Accepted: January 6, 2022
Published: January 27, 2022

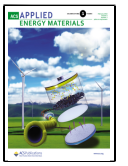

ments on γ-$Mg(BH_4)_2$.[10] To date, these characteristics have not proved advantageous as the metastable porous material displays many of the shortcomings of the α- and β-$Mg(BH_4)_2$ polymorphs.[11,12]

Many of the approaches aimed at mitigating poor dehydrogenation kinetics and cyclability of $Mg(BH_4)_2$ involve the use of additive compounds and molecules. Previous investigations have relied largely on mechanochemical and wet-chemical methods for introducing additives to borohydride compounds. The extreme reactivity of borohydrides (i.e., strong reducing capabilities) with a variety of materials makes the introduction of solvents particularly challenging. Additionally, solution-based processing can introduce undesirable solvent molecules, which become trapped in the porous network of γ-$Mg(BH_4)_2$. Conversely, it is noteworthy that solvent-based methods for synthesizing Lewis base complexes of ($Mg(BH_4)_2$) (e.g., $Mg(BH_4)_2$·THF (tetrahydrofuran) adducts) have demonstrated considerable improvements in kinetics with selectivity toward thermodynamically desirable intermediates/products, such as $B_3H_8^-$.[13] The success demonstrated by this systematic approach for uncovering the influence of relative strength of Lewis bases on the performance of $Mg(BH_4)_2$ is the inspiration for the approach used in the current study.

Mechanochemical approaches for modifying the properties of complex hydrides employ physical grinding or ball-milling in order to facilitate mixing or induce a reaction between the additive and hydride. These types of processes can introduce impurities (e.g., from the bearings/mill), induce complete amorphization, and initiate undesirable side reactions. Metals and metal halides are overwhelmingly favored as additives in mechanochemical-based methods for improvement of hydrogen release in borohydrides.[14−18] Recent work by Zhang and co-workers[15] examined the influence of metal fluorides MF_x (M = Zn, Ca, and Ti) and reported hydrogen release as low as 50 °C, but with a total H_2 capacity less than half the starting $Mg(BH_4)_2$ material. Most recently, Heere et al.[19] surveyed the influence of Nb_2O_5 and ball-milling on isotopic exchange—a metric used to estimate solid-state proton diffusion—and hydrogen release from γ-$Mg(BH_4)_2$. Although Nb_2O_5 additives show some improvements, the authors observed a considerable loss of specific surface area (SSA) and lowering of the structural phase transformation temperatures upon ball milling. After annealing the ball-milled sample, only 50% of the original SSA was recovered, highlighting the damaging structural effects of mechanical mixing on γ-$Mg(BH_4)_2$ and the need to separate the contributions of milling from the additive. The results reported by Li et al.[18] suggest that ball-milling α-$Mg(BH_4)_2$ without additives causes amorphization, but does not cause loss of hydrogen. However, when milled under identical conditions in the presence of various additives with a 1:3 weight ratio, up to ∼30% of the native hydrogen capacity is removed.

Here, we present a new vapor-phase additive approach derived from atomic layer deposition (ALD) designed to: (1) lower the temperature of hydrogen release in $Mg(BH_4)_2$ by enabling alternative decomposition routes potentially leading to milder rehydrogenation conditions, (2) prevent or minimize degradation of the $Mg(BH_4)_2$ crystalline structure during processing, and (3) expand the arsenal of useful additives beyond metals/metal halides and common solvents. Enhanced kinetics are also desirable, but direct comparison with untreated $Mg(BH_4)_2$ is often non-trivial due to alternate decomposition pathways and non-parallel rate processes. In this study, structure−function relationships were derived using a host of experimental characterization techniques. Powder X-ray diffraction (pXRD), small-angle scattering with simultaneous wide-angle X-ray scattering (SAXS-WAXS), diffuse reflectance infrared spectroscopy (DRIFTS), and Raman spectroscopy were used to provide information about the structure and dynamics of crystalline and amorphous species. Temperature-programmed desorption (TPD) and differential scanning calorimetry (DSC) measurements were necessary to characterize the thermodynamics of decomposition processes and evolution of gaseous products as a function of temperature. Proton-decoupled ^{11}B solid-state magic angle spinning nuclear magnetic resonance ($^{11}B\{^1H\}$ NMR) was used to illuminate changes in the local boron structure upon introduction of the vapor-phase additives. The vapor-phase additives (vapors from liquids and sublimates from solids) used in this study were introduced in an ALD chamber. The relative mole fraction of the additive can be precisely controlled with the number of pulses and pulse duration. In addition, infiltration into the γ-phase mesopore network is possible through changes in the additive molecular size and/or coordinating ligands. In the current study, we investigated the reactivity and efficacy of four additives: boron tribromide (BBr_3), trimethylaluminum (TMA) ($Al_2(CH_3)_6$), titanium tetrachloride ($TiCl_4$), and hydrazine (N_2H_4) toward improving hydrogen storage properties of γ-phase ($Mg(BH_4)_2$) using a vapor-phase method. The range of molecular species (e.g., boron trihalide, metal halide, and organoaluminum) and their inherent electrophilicities (from Lewis acid to base) among this set of additives presents a unique opportunity to conduct a systematic examination, whereby exposure and decomposition reactivities can be explored as a function of electronic structure. This unique approach should open the door to a new class of molecular additives and catalysts, which cannot easily be introduced with conventional mechanochemical- or solvent-based techniques.

EXPERIMENTAL SECTION

Sample Preparation. γ-Phase $Mg(BH_4)_2$ was synthesized using a procedure outlined by Zanella et al.[20] In short, dibutylmagnesium was added dropwise to borane-dimethyl sulfide dissolved in toluene at room temperature. The resulting precipitate was collected and dried under vacuum at 60 °C, which yields γ-phase $Mg(BH_4)_2$ with only trace quantities of α-$Mg(BH_4)_2$ upon desolvation.

Additive Exposure. Additive exposure was carried out in a commercial Beneq TFS 200 ALD reactor at temperatures between 30 and 50 °C in order to prevent loss of hydrogen from the $Mg(BH_4)_2$ material. A thin layer (∼50 mg, <1 mm thick) of the $Mg(BH_4)_2$ powder samples was enveloped into a tight stainless steel mesh and transferred air-free from a nitrogen glovebox into the ALD deposition chamber which was evacuated to reach a base pressure of ∼1 mTorr. Boron tribromide (BBr_3) and titanium tetrachloride ($TiCl_4$) were purchased from Strem Chemicals. TMA and anhydrous hydrazine (N_2H_4) were purchased from MilliporeSigma. The anhydrous N_2H_4 was further dried over CaH_2 and subsequently filtered in an inert atmosphere. In order to maintain a nominally uniform exposure among the various additives, 100 pulses were performed for each additive−$Mg(BH_4)_2$ combination, with pulses lasting 8 s each. Three minute nitrogen gas purges were conducted in between pulses. To accommodate the surface area of the powder substrate, the pulse duration for each cycle step was extended compared to ALD processes on flat substrates.

Structure and Dynamics Characterization. Synchrotron X-ray characterization of the additive−borohydride samples was performed

https://doi.org/10.1021/acsaem.1c03128
ACS Appl. Energy Mater. 2022, 5, 1690−1700

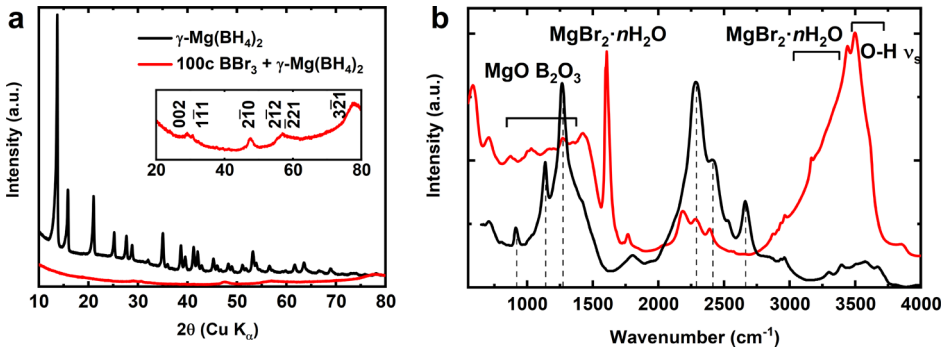

Figure 1. pXRD (a) and DRIFT spectra (b) of the γ-$Mg(BH_4)_2$ material before (black) and after (red) exposure to 100 pulses of BBr_3. The pXRD inset shows a magnified view of the region consistent with $MgBr_2$ and associated $MgBr_2$ Miller indices. The dashed lines in the DRIFT spectrum identify the locations of $Mg(BH_4)_2$ bending and stretching modes.

at the Stanford Synchrotron Radiation Lightsource (SSRL, SLAC). SAXS-WAXS measurements were conducted at beam line 1−5 (λ = 0.7999 Å). For both sets of measurements, powder samples were prepared in ø 1 mm (10 μm wall thickness) quartz capillaries inside an argon glovebox. The capillaries were subsequently loaded into a capillary heating sample cell described elsewhere.[21] The sample cell was sealed, removed from the glovebox, and connected to a gas-handling manifold. In situ X-ray scattering measurements were conducted under dynamic vacuum with a base pressure of 10 mTorr.

Lab-source X-ray diffraction measurements were conducted on a PANalytical Empyrean diffractometer using incident Cu Kα radiation (λ = 1.54 Å) in line mode, 1° antiscatter slit, 20 mm divergent height limiter slit, and 0.25° divergence slit on the incident beam. The hybrid pixel detector with fixed antiscatter slits was mounted onto the goniometer with a radius of 240 mm. The XRD samples were prepared in quartz capillaries with a 1 mm diameter and a 10 μm wall thickness that were sealed with paraffin wax.

Solid-state MAS ^{11}B NMR measurements were performed on a Bruker AVANCE III 400 MHz at room temperature using a 4 mm magic angle spinning double resonance probe. The probe was operated in the X-BB mode and was spinning at 14 kHz. The ^{11}B direct polarization experiments were executed with a 5 s delay time and the ^{1}H−^{11}B cross polarization (CP) experiments with a contact time of 2000 μs. The NMR probes were tuned to 128.3928 MHz for ^{11}B and 400.2059 MHz for ^{1}H, respectively. The rotors were filled and sealed with an air-tight cap in an inert atmosphere prior to the measurement. BF_3−OEt_2 was used as an external reference.

Solid-state MAS ^{27}Al NMR measurements were performed on an Agilent VNMRS 500 MHz at ambient temperature using a homebuilt 5 mm double resonance probe with a Vespel housing. The sample was packed into a 5 mm zirconia cavern style rotor designed for sealing samples under inert gas or for high-pressure work.[22] The pulse sequence was a Hahn spin echo[23] to try and minimize any ^{27}Al background signal originating from the probe head; however a difference experiment was still required due to the presence of aluminum in the ZrO_2 rotor as a stabilizing agent. The RF fields utilized were near 50 kHz for ^{27}Al and 35 kHz for ^{1}H during SPINAL-64[24] decoupling. Recycle delay was 1 s for a total experiment time of 18 h (for each).

DRIFTS measurements were collected on a Nicolet 6700 with a liquid nitrogen cooled MCT (HgCdTe) detector using a Harrick Scientific Praying Mantis Diffuse Reflectance Accessory. All samples were mixed with potassium bromide (dehydrated in a vacuum oven at 200 °C and stored in an inert atmosphere) with the resulting mixture being a 10 wt % sample. The sample was then loaded into the DRIFTS chamber in a glovebox and transferred air-free to the Nicolet 6700. The area between the DRIFTS accessory and the detector was purged with nitrogen gas. For each spectrum collected, neat KBr was used as a background and 1020 scans were averaged.

Thermal Decomposition Characterization. Using a custom-built TPD instrument,[25] the additive−$Mg(BH_4)_2$ materials were heated from room temperature to 500 °C with a 15 °C/min ramp rate using a Digi-Sense temperature controller. The rate of temperature increase was chosen such that the released hydrogen did not alter the evacuation rate of the system. The gas-phase species released during heating were analyzed using a Stanford Research Systems Residual Gas Analyzer (RGA) 100 at a 70 eV ionization energy, scanning m/z = 1−50 amu at a sampling rate of 2−4 s. A LabVIEW-based GUI was used to control all experimental parameters. In order to optimize both the m/z = 2 (H_2) signal and instrumental dynamic range, the amount of sample was varied between 1 and 2 mg. The resulting RGA signal was normalized to the starting sample mass. Powders were packaged in Pt foil to facilitate uniform heating and were subsequently sealed in a quartz tube mounted to the TPD instrument. The quartz tube was evacuated prior to heating until a pressure of at least 10^{-8} Torr and no m/z-signal above background was observed, with special scrutiny on water, air, and hydrogen. Upon reaching 500 °C, the temperature was maintained for 1 h to ensure full dehydrogenation was achieved. The total gravimetric H_2 capacity, with an accuracy of ±10%, was calculated by numerically integrating the signal of m/z = 2 over the total measurement time. The mass-normalized signal was scaled by the well-established H_2 capacity of TiH_2 (4.0 wt % H_2). To this end, reference TiH_2 (Alfa Aesar, 99%) TPD measurements were obtained under conditions identical to the additive−$Mg(BH_4)_2$ samples.

DSC measurements were performed on a Q20 TA Instrument differential scanning calorimeter in a nitrogen atmosphere from 25 to 500 °C with a heating rate of 15 °C/min. The samples were enclosed in hermetically sealed aluminum (Al) pans prepared in a He glovebox. Empty reference Al pans were prepared under identical conditions.

RESULTS AND DISCUSSION

Boron Tribromide. The first additive investigated among a series of vapor-phase precursors involved the exposure of 100 pulses of BBr_3 to a sample of γ-$Mg(BH_4)_2$. Although somewhat counterintuitive based on electronegativity and steric limitations, Lewis acidity is strongest in BBr_3 relative to the chloride and fluoride boron trihalides.[26] A strong reaction between BBr_3 and $Mg(BH_4)_2$ occurs during initial additive exposure as indicated by the substantial structural changes to the starting γ-phase $Mg(BH_4)_2$ material. Structural degradation was detected using the pXRD and DRIFTS results in Figure 1a,b, before and after 100 pulses of BBr_3.

The diffraction pattern from the γ-$Mg(BH_4)_2$ sample prior to additive exposure exhibited reflections exclusively from the highly crystalline cubic structure.[9] All diffraction peaks from the initial γ-$Mg(BH_4)_2$ material were noticeably absent in the pXRD pattern after 100 pulses of BBr_3, which indicated the initial cubic $Mg(BH_4)_2$ crystal structure became highly disordered or decomposed altogether. Following exposure to BBr_3. A few broad, weak diffraction peaks (shown in the magnified inset) were observed and are consistent with the

https://doi.org/10.1021/acsaem.1c03128
ACS Appl. Energy Mater. 2022, 5, 1690−1700

most intense reflections of $MgBr_2$[27] present at 2θ = 30.6 (0 0 2, 1 $\bar{1}$ 1) 47.7 (2 $\bar{1}$ 0), 57 (2 $\bar{1}$ 2, $\bar{2}$ 2 1), and 77.9° (3 $\bar{2}$ 1). DRIFTS measurements provide additional clarity on the identity of non-crystalline reaction products and are advantageous for these samples because there is a higher sensitivity toward surface species, relative to transmission-based techniques. In DRIFTS sampling, both surface and bulk signals are captured simultaneously. The vibrational modes of $Mg(BH_4)_2$ are well characterized and are described in detail elsewhere.[28−30] The two DRIFT spectra in Figure 1b illustrate a dramatic reduction of B−H bending (δ) and stretching (ν) modes, characteristic of $Mg(BH_4)_2$, at δ = 1137 (m), 1266 (s) and ν = 2290 (s), 2418 (m), and 2666 (m) cm^{-1}, upon exposure of $Mg(BH_4)_2$ to BBr_3. This abrupt loss of the signal from $Mg(BH_4)_2$ was also observed in the complementary Raman spectrum (see Figure S1). Unfortunately, the energy window of the DRIFT spectrometer is too high to observe lattice modes from $MgBr_2$ and MgB_2, which would provide direct evidence of their formation. However, O−H bending and stretching modes are identified in the DRIFTS from a hydrate of $MgBr_2$ at δ = 1600 (s) and a broad band above ν = 3000 (s) cm^{-1}, respectively.[31] Absorption bands are also identified in spectral regimes consistent with vibrational modes from hydroxide (broad band at ν = 3450 (s) cm^{-1})[27] and other oxide species, such as magnesium borates.[32] Although the surfaces of the $Mg(BH_4)_2$ particles are known to display native oxides,[33] their relative abundance is low enough such that little-to-no oxide/hydroxide or hydrate signal was observed in the DRIFTS from γ-$Mg(BH_4)_2$ prior to additive exposure. Following the exposure of BBr_3 (and all subsequently studied additives) to $Mg(BH_4)_2$, there were spectral indications of oxide and hydrate species, which suggest that the "air-free" sample transfer or chamber used for additive exposure introduced trace amounts of oxygen and/or water, which are known to cause rapid hydrolysis or surface oxidation.[34] The formed surface oxides are a potential source of non-volatile reaction products, which explains their increased relative contribution in the post-exposure DRIFTS measurements.

$^{11}B\{^1H\}$ SS NMR measurements in Figure 2 lend further support to the observed reactivity of the borohydride environment with BBr_3. For the BBr_3-treated $Mg(BH_4)_2$ sample, the BH_4^- environment is identified by a peak located at (400 MHz, BF_3OEt_2, δ): −40 ppm for $Mg(BH_4)_2$. A second, less-abundant, boron environment is detected by a peak located at approximately (400 MHz, BF_3OEt_2, δ): −34 ppm following exposure to BBr_3. A peak with this chemical shift does not coincide with any of the commonly occurring polyboranes[35] and is potentially a partially brominated borohydride, where the electronegative bromide anion deshields the coordinating boron atom directing the borohydride chemical shift downfield from −40 ppm. The formation of the fully brominated anion species (e.g., BBr_4^-) is improbable because it is typically stabilized only by large cations.[36] Alternatively, Brown et al.[37] observed the formation of $HBBr_2S(CH_3)_2$ when BBr_3 was reacted with the borane adduct of dimethyl sulfide, which also cannot be ruled out as the cause of the peak at −34 ppm because residual dimethyl sulfide is known to be trapped in the pores of γ-$Mg(BH_4)_2$ during synthesis. Smaller peaks located near (400 MHz, BF_3OEt_2, δ): 14.5 and 0.9 ppm are also noted and correspond to borates/boric acid[38] and a four-coordinate B−O species,[39] respectively, which is consistent with the decomposition of $Mg(BH_4)_2$ and the presence of oxides in the pXRD pattern and DRIFTS spectra in Figure 1.

TPD measurements on the BBr_3−$Mg(BH_4)_2$ sample heated to 500 °C (see Figure S2) indicate that only 0.3 H_2 wt % remains in the sample after exposure of BBr_3 providing evidence that most of the initial hydrogen content is lost during pulsing. Although BBr_3 is also known to react in excess H_2 to produce HBr, there is no evidence of HBr formation (physisorbed or pore-confined) or corresponding yield of elemental boron to support this alternate reaction pathway. Furthermore, because $MgBr_2$ is observed, HBr is not expected to form in an appreciable quantity. The extreme reactivity of BBr_3 with $Mg(BH_4)_2$ during pulsing suggests that it is unsuitable for use as a molecular additive. However, the formation of $MgBr_2$ and the absence of hydrogen in the TPD results clearly demonstrate that hydrogen (or a hydrogen-bearing species) is rapidly evolved during the gas-phase reaction with the additive, which is a property that may be investigated and possibly exploited in subsequent studies.

Trimethylaluminum. TMA is another electrophilic additive but is a weaker Lewis acid than BBr_3. The TPD results from the 100 pulse TMA-γ-$Mg(BH_4)_2$ sample, provided in Figure 3, indicate that rapid release of hydrogen occurs

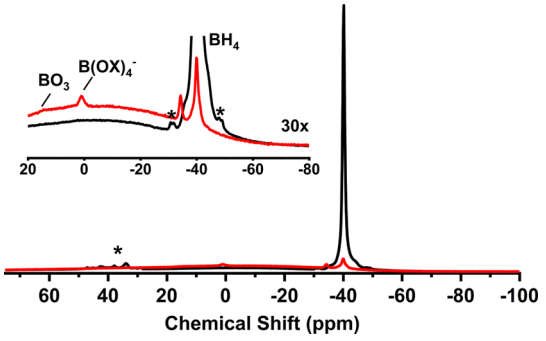

Figure 2. $^{11}B\{^1H\}$ SS-NMR spectra of the γ-$Mg(BH_4)_2$ sample before (black) and after (red) exposure to 100 pulses of BBr_3. The inset provides a magnified view of the unknown boron environment at −34 ppm. The asterisks denote the locations of spinning sidebands.

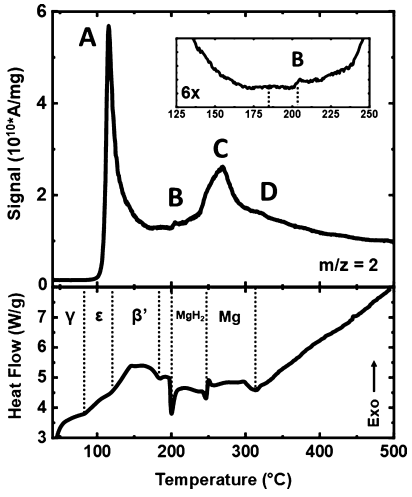

Figure 3. TPD (top) and DSC (bottom) data from γ-$Mg(BH_4)_2$ exposed to 100 pulses of TMA. The hydrogen release events (A−D) in the TPD are accordingly traced to some of the features in the DSC via the dotted lines.

https://doi.org/10.1021/acsaem.1c03128
ACS Appl. Energy Mater. 2022, 5, 1690−1700

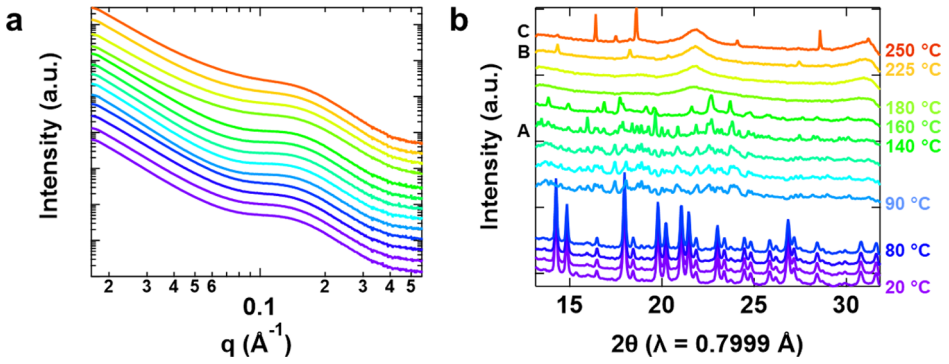

Figure 4. In situ temperature-resolved SAXS (a) and WAXS (b) measurements on the 100 pulse TMA + γ-$Mg(BH_4)_2$ material. Patterns are manually offset for clarity. The sequential coloring represents the temperature and is identical in both sets of patterns. Events A-C from the TPD/DSC are labeled on the WAXS y-axis.

between 95 and 115 °C, which is well below the decomposition temperature of $Mg(BH_4)_2$. The temperature of this desorption event coincides with the temperature associated with the release of pore-confined dimethyl sulfide and suggests that TMA infiltrates the porous γ-phase structure, which is consistent with behavior observed in prior work.[34] Another feature (event C), corresponding to a more prominent release of hydrogen, was observed between 240 and 260 °C. DSC measurements with identical heating rates show endothermic features in the vicinity of the hydrogen release temperatures (events A, C in Figure 3).

Although the total hydrogen content released between room temperature and 500 °C amounted to less than 20% (2.5 H_2 wt %) of the total γ-$Mg(BH_4)_2$ theoretical H_2 capacity (~14.9 H_2 wt %), the dramatic reduction of decomposition temperature and combined rapid release of hydrogen in the crystalline structural regime shown in Figure 3 stimulated interest in the reaction mechanism. In order to further understand the decomposition process and how TMA pore infiltration may play a role in the material degradation, in situ temperature-resolved SAXS-WAXS measurements were performed, as shown in Figure 4a,b. The SAXS signal in Figure 4a indicates the inherent porosity of the γ-$Mg(BH_4)_2$ structure remains after exposure to TMA as indicated by the Guinier shoulder near $q \sim 0.15$ Å^{-1}, corresponding to a pore size of about 40 Å. This feature remains in the SAXS pattern throughout the entire temperature series, which may suggest the TMA facilitates residual porosity in $Mg(BH_4)_2$ during decomposition leading to structural instability. The corresponding WAXS signal shows the TMA-exposed material remains predominantly in the γ-phase, which is not observed in other additive–$Mg(BH_4)_2$ studies. Between 80 and 90 °C (event A in the TPD/DSC), the material undergoes the well-known structural phase transformation into ε-phase $Mg(BH_4)_2$, which is ~30 °C lower than observed for the neat material. The ε- to β-phase structural transformation is noted between 140 and 160 °C. Interestingly, reflections from the β-phase, which are typically not observed at maximum until ~180 °C, disappear completely between 160 and 180 °C in concert with an endothermic feature (event B) in the DSC. The lowering of the β-$Mg(BH_4)_2$ decomposition temperature suggests that the TMA's reaction product has a destabilizing effect on the borohydride crystal structure. A diffraction pattern with only a few broad peaks persists until ~225 °C, where MgH_2 is identified as the primary crystalline constituent. By 250 °C, MgH_2 is converted to the Mg metal (event C in TPD/DSC), a process again occurring at 30 °C lower than in the neat $Mg(BH_4)_2$ material under vacuum.

The considerable signal from crystalline γ-$Mg(BH_4)_2$ remaining in the WAXS pattern following exposure of TMA indicates that the reaction does not propagate into the bulk structure. From the data presented above, it is reasonable to assert that the TMA additive and its reaction products are confined to the surface or pores of $Mg(BH_4)_2$. ^{27}Al SS NMR measurements (shown in Figure S3) indicate only minute quantities of aluminum remain in the 100-pulse sample (i.e., the highest additive concentration) and appear with chemical shifts in the vicinity of aluminum oxides. TPD from a recent study[34] highlighting the impact of ALD alumina coatings on decomposition of $Mg(BH_4)_2$ shows hydrogen release at distinctly higher temperatures than the 100-pulse TMA sample in this work and suggests that the residual alumina species observed in the ^{27}Al SS NMR are unlikely responsible for the marked destabilization of $Mg(BH_4)_2$. DRIFT spectra displayed in Figure 5 show a broad increase in absorption between 1000

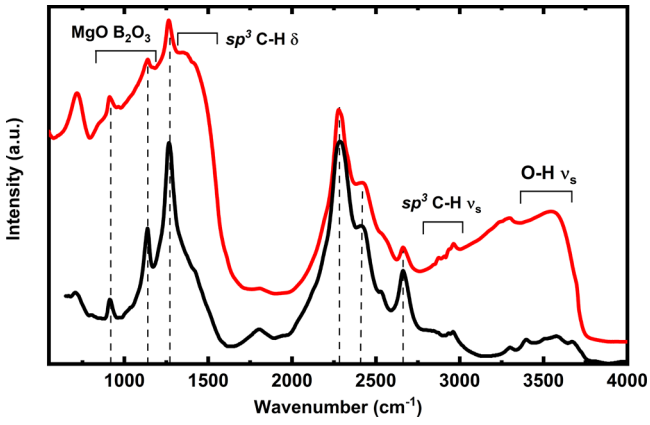

Figure 5. Comparison of the DRIFT spectra between 100 pulse TMA + γ-$Mg(BH_4)_2$ (red) and γ-$Mg(BH_4)_2$ (black). The dashed lines in the DRIFT spectrum identify the locations of $Mg(BH_4)_2$ bending and stretching modes.

and 1500 cm^{-1}, which is in the vicinity of sp^3 C–H bending modes signifying the presence of methyl groups following exposure of TMA. This observation is supported by TPD results, which also reveal a small amount of CH_4 (see Figure S4) released near 200 °C. The presence of oxides/hydroxides is also noted in the DRIFTS near 1000 and above 3000 cm^{-1}. The B–H bending (δ = 1080 (w) cm^{-1}) and stretching (ν =

https://doi.org/10.1021/acsaem.1c03128
ACS Appl. Energy Mater. 2022, 5, 1690–1700

2150, 2236, 2300 (s) cm^{-1}) modes of $Mg(BH_4)_2$ appear to be minimally influenced by TMA exposure, confirming the integrity of the remaining BH_4^- species shown previously in the WAXS. Unfortunately, the related Raman spectrum for the TMA-exposed $Mg(BH_4)_2$ exhibited a strong fluorescence signal (see Figure S5), which made the data unusable. However, the corresponding $^{11}B\{^1H\}$ SS-NMR spectrum (Figure S6) exhibits only contributions from BH_4^- (−40 ppm), $B(OH)_4^-$ (2 ppm), and borates (14 ppm). The absence of additional boron environments indicates that the decrease in decomposition temperature is also unrelated to boron-containing species. With no evidence of active aluminum or boron species, the destabilizing component must result from a reaction, where BH_4^- and CH_3 groups are left intact. We suggest that an exchange reaction between $Mg(BH_4)_2$ and TMA occurs forming $MgBH_4CH_3$ or $Mg(CH_3)_2$, which would be difficult to isolate and characterize with structural or dynamics techniques due to the disordered or polymeric natures of such species. It is assumed that these species are converted to nanostructured MgH_2 (in the presence of excess H_2) above 200 °C, where CH_4 is observed in the TPD. This type of behavior has also been observed for Grignard reagents, such as CH_3MgBr.[40] To the best of our knowledge, this is the first report that describes the use of an Al-based additive to destabilize $Mg(BH_4)_2$. The remarkable findings outlined above warrant additional investigations of Al-based additives for further improving the destabilization of $Mg(BH_4)_2$.

The hydrogen release properties of the TMA-exposed $Mg(BH_4)_2$ sample were also explored as a function of additive pulse number in an attempt to exploit the lowering of the decomposition temperature while maintaining a high hydrogen capacity. TPD measurements comparing the performance of γ-$Mg(BH_4)_2$ to that with 10 and 100 pulses of TMA are shown in Figure 6. For the neat sample of γ-$Mg(BH_4)_2$, the first

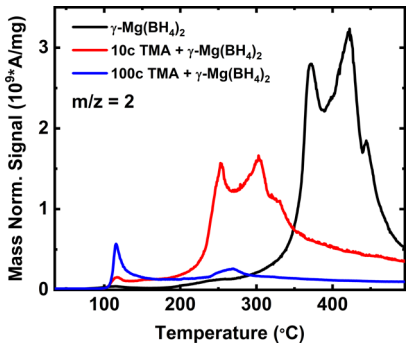

Figure 6. TPD data showing hydrogen release ($m/z = 2$) as a function of temperature and TMA pulses for γ-$Mg(BH_4)_2$ (black), 10 pulses TMA + γ-$Mg(BH_4)_2$ (red), and 100 pulses TMA + γ-$Mg(BH_4)_2$ (blue).

prominent peak corresponding to the evolution of hydrogen is not observed until ∼350 °C. Exposure to 100 pulses of TMA enhances the hydrogen released at ∼115 °C and lowers the primary release to 250 °C (100 °C lower than the neat material), but reduces the total hydrogen content to only 2.5 H_2 wt % (only 17% of the theoretical value for $Mg(BH_4)_2$). Remarkably, when the number of pulses is reduced from 100 to 10, the primary hydrogen release event is still observed at 250 °C, but the total hydrogen capacity was increased to 14.47%, which is 97% of the theoretical value. As a result, a reduction in the number of TMA pulses results in the ability to prevent loss of native hydrogen content while retaining the low temperature of hydrogen release, which is a property unique to this vapor-phase approach.

Titanium Tetrachloride. Titanium-containing compounds have been extensively investigated as additives because of their demonstrated success in a variety of catalytic reactions.[41] As a transition metal, titanium exhibits three known oxidation states, which can accommodate charge balance, changes in the coordination number, and formation of metastable intermediates in a number of chemical environments encountered during decomposition reactions. Prior work[15,17] has indicated that titanium-based additives facilitate reasonable improvements in the decomposition of complex hydrides (e.g., lowered decomposition temperatures and faster hydrogen release), though with a limited understanding of the mechanism. Titanium tetrachloride is an interesting additive because its effect on $Mg(BH_4)_2$ had yet to be explored and it is a strong Lewis acid that can undergo exothermic reactions with bases to yield $TiCl_y$-X_z adducts.[36] In this investigation, 100 pulses of $TiCl_4$ were introduced to a sample of γ-$Mg(BH_4)_2$. Structural modifications to the starting material upon exposure to $TiCl_4$ are shown in Figure 7a,b. The pXRD pattern indicates that the bulk γ-phase structure is marginally influenced by the $TiCl_4$ additive. However, new broad, amorphous contributions identified in the pXRD are observed across three different q-ranges shown in the inset of Figure 7a. Additionally, β-phase $Mg(BH_4)_2$ was identified in the additive mixture, which provides supporting evidence for an exothermic reaction accompanied by sample heating. The DRIFT spectra presented in Figure 7b show the preservation of peaks related to $Mg(BH_4)_2$ vibrational modes, described previously, following exposure of $TiCl_4$. As was the case for the BBr_3-exposed sample, hydrate modes from a metal halide hydrate are observed near ν = 1600 (w) and above ν = 3000 (m) cm^{-1}.[42] However, in contrast to the BBr_3 exposure, $MgCl_2$ appears to be limited to the surface regions of $Mg(BH_4)_2$ because the γ-phase reflections and BH_4^- vibrational modes are visible in the pXRD pattern and DRIFTS/Raman spectra (Figures 7b and S7), respectively. TPD results provided in Figure 8 indicate that the release of hydrogen follows a mechanism similar to neat γ-$Mg(BH_4)_2$ (e.g., three primary hydrogen release events), decreasing the decomposition temperature by about 50 °C, though with a total H_2 wt % of only 5.7%. A comparison can be made with the results from Newhouse et al.,[14] which demonstrated that 5 mol % TiF_3 + $ScCl_3$ ball-milled with α-$Mg(BH_4)_2$ yields an increased amount of H_2 released near 300 °C, seemingly from a MgH_2 thermal decomposition product destabilized by polyborane intermediates formed at low temperatures. It was previously conjectured that the substitution of halides into a borohydride lattice can potentially reduce the binding energy between the metal and the BH_4^- group.[43] However, the addition of halides with Van der Waal radius less than that of the borohydride (e.g., Cl^-, Br^-) to $Mg(BH_4)_2$ have shown only modest reductions of decomposition temperatures (ΔT < 30 °C) over the neat $Mg(BH_4)_2$ sample. The exposure of $TiCl_4$ to $Mg(BH_4)_2$ appears to have a more pronounced effect on lowering the decomposition temperature in comparison to these similar additive mixtures with hydrogen release first observed near 150 °C and the first prominent release event below 300 °C.

Currently, there is no available literature on the reaction between $Mg(BH_4)_2$ and $TiCl_4$. However, when reacted with excess $LiBH_4$, $TiCl_4$ reportedly produces $Ti(BH_4)_3$,[44] which is

https://doi.org/10.1021/acsaem.1c03128
ACS Appl. Energy Mater. 2022, 5, 1690−1700

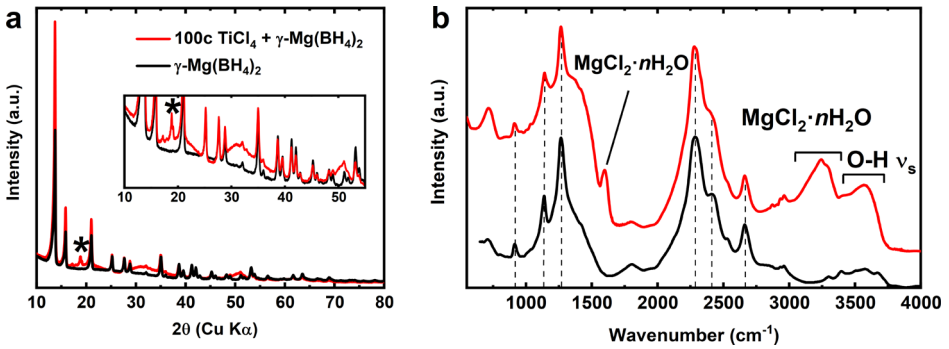

Figure 7. pXRD (a) and DRIFT spectra (b) of the γ-$Mg(BH_4)_2$ material before (black) and after (red) exposure to 100 pulses of $TiCl_4$. The asterisk in the XRD data denotes the location of the 022 reflection (i.e., the most prominent diffraction peak) of β-$Mg(BH_4)_2$. The dashed lines in the DRIFT spectrum specify the locations of $Mg(BH_4)_2$ bending and stretching modes.

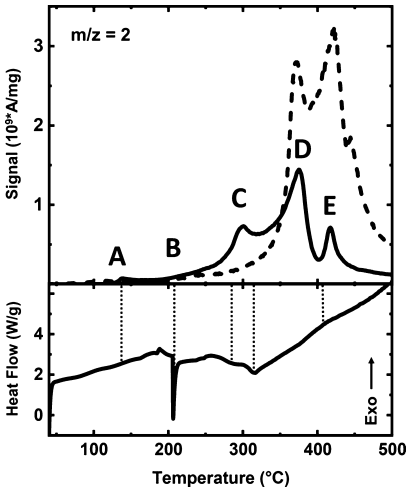

Figure 8. TPD (top) and DSC (bottom) data from γ-$Mg(BH_4)_2$ exposed to 100 pulses of $TiCl_4$. The hydrogen release events (A–E) in the TPD are accordingly traced to features in the DSC via the dotted lines. The TPD signal from neat γ-$Mg(BH_4)_2$ is shown by the dashed trace.

unstable at room temperature and decomposes rapidly to TiB_2 (or other Ti_xB_y species). In contrast, the reaction between $Al(BH_4)_3$ and $TiCl_4$ yields $TiCl(BH_4)_2$ and $AlCl_2BH_4$ with simultaneous formation of B_2H_6 and H_2. The absence of TiB_2 (or any other titanium–boron environments) in the Raman spectrum or ^{11}B NMR from the $TiCl_4$-exposed material (see Figures S7 and S8, respectively) suggests that $Ti(BH_4)_3$ is not produced, effectively ruling out the former route. A more plausible reaction mechanism for $TiCl_4$-exposed $Mg(BH_4)_2$ is one analogous to that of $Al(BH_4)_3$, where a distribution of substituted products are formed. Recognizing evidence of $MgCl_2$ in the DRIFTS, the predicted reaction should involve the exchange of at least two chlorides between $Mg(BH_4)_2$ and $TiCl_4$, which suggests both $MgClBH_4$ (i.e., the partially substituted species) and $MgCl_2$ are conceivable products. The corresponding $TiCl_{4-x}(BH_4)_x$ species are seemingly volatile because there is little evidence of a titanium-containing species in the DRIFTS or ^{11}B NMR. In a similar "co-additive" system with 100 alternating pulses of $TiCl_4$ and N_2H_4, transmission electron microscopy with energy dispersive X-ray spectroscopy provided supporting evidence that chlorine (3.9%) was concentrated near the particle surface and the titanium content (0.6%) was minimal.[45] As a result, it is suspected that lowering of the onset temperature for hydrogen release from $TiCl_4$-exposed $Mg(BH_4)_2$ is related to reduced crystallite sizes as the proposed reaction removes surface atoms and the presence of surface-restricted $MgClBH_4$ or $MgCl_2$ species, which facilitate the decomposition of $Mg(BH_4)_2$.

Hydrazine. Hydrazine presents another opportunity for enhancing the decomposition properties of $Mg(BH_4)_2$, distinct from those described previously. Of all the additives discussed, hydrazine is the only molecule that is nucleophilic. The primary incentive for using a nucleophile was that the electron-abundant environment of the additive would decrease reactivity during exposure, allowing for a greater number of pulses (and hence more additive molecules) with simultaneous preservation of the native hydrogen content in $Mg(BH_4)_2$. Another benefit of hydrazine relative to the other additives is the introduction of mixed hydridic/protonic hydrogen species. Previous examinations of a hydrazine-borohydride system involved the interaction of α-phase $Mg(BH_4)_2$ with hydrazine vapor in a closed container.[46] After reacting with hydrazine overnight, the mixture was ball-milled, generating $(Mg(BH_4)_2)$ hydrazinate adducts. The authors suggested as much as 12.5 wt % H_2 is released from a $3Mg(BH_4)_2$–$4N_2H_4$ species at 240 °C. In contrast, TPD from our 100-pulse sample reveals only 4.8 wt % H_2 is released below 500 °C as depicted in Figure 9. The

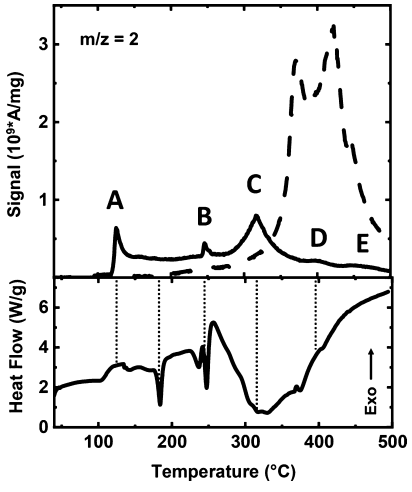

Figure 9. TPD (top) and DSC (bottom) data from γ-$Mg(BH_4)_2$ exposed to 100 pulses of N_2H_4. The hydrogen release events (A–E) in the TPD are accordingly traced to features in the DSC via the dotted lines. The TPD signal from neat γ-$Mg(BH_4)_2$ is shown by the dashed trace.

https://doi.org/10.1021/acsaem.1c03128
ACS Appl. Energy Mater. 2022, 5, 1690–1700

shape of the TPD signal for H_2 between room temperature and 500 °C is similar, but not identical to the results obtained by He et al., which may indicate that only a fraction of the product may convert to an $Mg(BH_4)_2$-nN_2H_4 adduct. It is also worth noting that differing experimental conditions may influence the preferred product of hydrazine reacted with $Mg(BH_4)_2$ (e.g., closed cell and long equilibration times of He et al. promoting the hydrazine adduct).

Interestingly, a subtle peak in the ^{11}B NMR (Figure 10) is observed near (400 MHz, BF_3OEt_2, δ): −22 ppm consistent

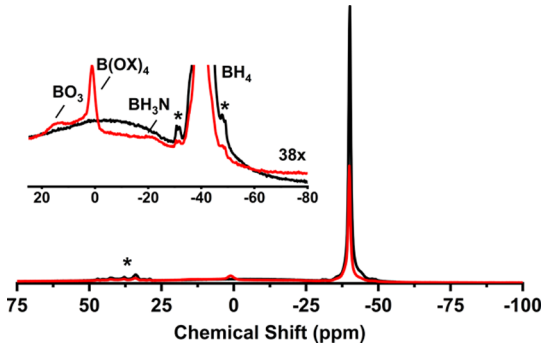

Figure 10. $^{11}B\{^1H\}$ SS-NMR spectra of the γ-$Mg(BH_4)_2$ sample before (black) and after (red) exposure to 100 pulses of N_2H_4. The inset provides a magnified view of the BH_3N environment at −22 ppm. The asterisks denote the locations of spinning sidebands.

with boron in a BH_3N environment.[47,48] Hydrazine with water contamination promotes the formation of hydrazine hydrate. In the hydrazinate crystal structure reported by He et al., hydrazine molecules are located at sites between Mg^{2+} and BH_4^-. It is anticipated that water bound to hydrazine (if not completely dehydrated) would cause rapid hydrolysis of the borohydride anion, resulting in the formation of hydrazine borane (or bis-borane), H_2, and Mg−OH species. A side reaction leading to hydrazine borane or a similar molecule would explain the presence of BH_3N species in the ^{11}B NMR,[49] low-temperature release of H_2 in the TPD (see Figure 9),[50−52] as well as the loss of hydrogen capacity during N_2H_4 exposure. Although this sample has not been ball-milled (as was the case for He et al.), pXRD measurements indicate that γ-$Mg(BH_4)_2$ is the only crystalline product, with a broad amorphous band visible at 2θ = 27° (see Figure 11a), which may indicate a weakly ordered or highly disordered structure.

The DRIFT spectrum, observed in Figure 11b, shows a reduction in the borohydride absorption bands after exposure to N_2H_4, but an increase in absorption near ρ/δ = 1000−1500 (s) and ν = 3260 (m) cm^{-1}, corresponding to N−H rocking/bending and stretching modes, consistent with hydrazine borane.[52] Spectral features indicative of hydrazine borane are also observed in the related Raman spectrum (see Figure S9). Also notable is the increase in O−H stretching from hydroxide and/or water as well as a new O−H bend around δ = 1600 (w) cm^{-1}. The absorption band present near ν = 3600 (m) cm^{-1} is consistent with the location of a hydroxyl stretching mode[53] but has also been observed in the reported infrared spectrum from hydrazine bis-borane.[54] Although these species are only present at low concentrations and likely confined to the surface of $Mg(BH_4)_2$, vapor-phase addition of hydrated N_2H_4 to $Mg(BH_4)_2$ opens up new opportunities to synthesize mixed protonic-hydridic hydrazine borane-coated borohydrides.

CONCLUSIONS

The introduction of additives to $Mg(BH_4)_2$ by precisely controlled pulses of reactive vapor-phase molecules represents an innovative approach for modifying the properties of complex hydrides, circumventing the need for mechanochemical mixing and wet-chemical techniques, which have a negative effect on the crystallinity and porosity of materials such as γ-$Mg(BH_4)_2$. It is not unexpected that most of the vapor-phase additives used in this study are considerably more reactive than their solid-phase analogues, especially considering their electrophilic character. A compilation of the hydrogen content for each additive−$Mg(BH_4)_2$ combination is shown below in Table 1. It was shown that for reactions leading to volatile

Table 1. Summary of Total Hydrogen Released below 250 and 500 °C for the Various Additive−$Mg(BH_4)_2$ Combinations

material	H_2 wt % released <250 °C	H_2 wt % released <500 °C
γ-$Mg(BH_4)_2$	0.37	14
γ-$Mg(BH_4)_2$ + 100 pulses BBr_3	0.06	0.28
γ-$Mg(BH_4)_2$ + 10 pulses TMA	1.5	14
γ-$Mg(BH_4)_2$ + 100 pulses TMA	1.1	2.5
γ-$Mg(BH_4)_2$ + 100 pulses $TiCl_4$	0.41	5.7
γ-$Mg(BH_4)_2$ + 100 pulses N_2H_4	1.5	4.8

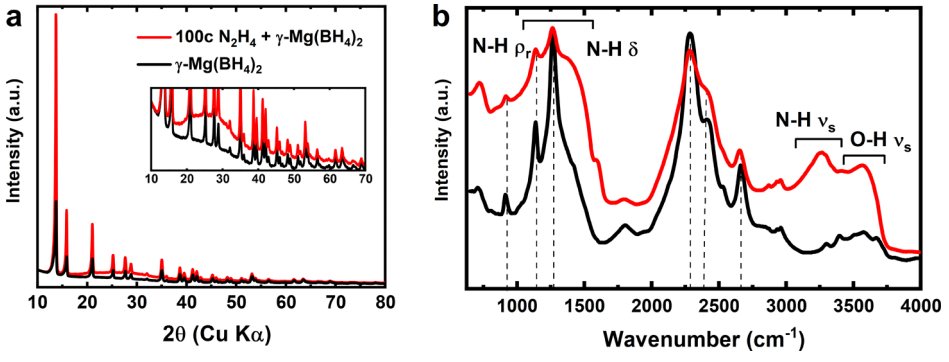

Figure 11. pXRD (a) and DRIFT spectra (b) of the γ-$Mg(BH_4)_2$ material before (black) and after (red) exposure to 100 pulses of N_2H_4. The inset in the pXRD pattern shows a magnified view of the amorphous contribution. The dashed lines in the DRIFT spectrum identify the locations of $Mg(BH_4)_2$ bending and stretching modes.

https://doi.org/10.1021/acsaem.1c03128
ACS Appl. Energy Mater. 2022, 5, 1690−1700

Table 2. Summary of Existing Methods for Destabilizing $Mg(BH_4)_2$

method	material	onset T_{dec} (°C)	ΔT_{dec} max. (°C)[a]	total H_2 wt %	refs
nanoconfinement	$Mg(BH_4)_2$ in activated carbon	150	12	6	55
solvent additive	$Mg(BH_4)_2 \cdot n$THF[b]			2.5	13
ball-milled additive	$TiCl_3/\alpha$-$Mg(BH_4)_2$ (1:3)[c]	88	110	10	18
hydride composite	$Mg(BH_4)_2$/LiH (2:1)	150	65	14.6	56
cation substitution	$Mg_{(1-x)}Zn_x(BH_4)_2$	125	100	7	57
vapor-phase additive	TMA on γ-$Mg(BH_4)_2$	115	100	14.7	this work

[a]All "ΔT_{dec} max." values determined relative to the respective $Mg(BH_4)_2$ control measurement reported in each study. [b]No quantitative analysis of decomposition. Intentionally formed MgH_2 + $Mg(B_3H_8)_2$. [c]Claim pure hydrogen, but only thermogravimetric analysis data provided.

reaction products, which desorb and lead to non-self-terminating behavior, reducing the number of pulses prevents the loss of native hydrogen while retaining the "destabilizing" influence of the additive. This effect was demonstrated by lowering the number of pulses from 100 to 10 in the TMA-$Mg(BH_4)_2$ system. The 10-fold decrease in the amount of TMA pulses leads to a 100 °C reduction (relative to the neat γ-$Mg(BH_4)_2$ sample) in the first prominent release of hydrogen and a total hydrogen capacity of 14 H_2 wt %, which is greater than 97% the theoretical gravimetric capacity of $Mg(BH_4)_2$. It is also worth noting that both the 10 pulse TMA-$Mg(BH_4)_2$ and 100 pulse N_2H_4–$Mg(BH_4)_2$ samples released four times as much hydrogen below 250 °C than from the neat $Mg(BH_4)_2$ material. The identity of the boron species in these two mixtures at 250 °C will be emphasized in a follow-up study in an attempt to demonstrate reaction reversibility (i.e., rehydrogenation) for the high-performing additive–$Mg(BH_4)_2$ materials.

A comparison of performance between the vapor-phase TMA additive and other leading methods used for destabilization of $Mg(BH_4)_2$ is provided in Table 2. The TMA-exposed $Mg(BH_4)_2$ sample exhibits hydrogen release properties, which rival or exceed other methods available in the literature on the basis of onset temperature for hydrogen release, a shift in temperature of maximum hydrogen release, and total hydrogen wt % from $Mg(BH_4)_2$ released below 500 °C.

Using this alternative approach to destabilization of complex hydrides, a series of molecular additives with a range of electronic properties were systematically investigated in order to examine the influence of central atom nucleophilicity/electrophilicity on temperature-limited H_2 release from $Mg(BH_4)_2$. The order of initial exposure reactivity observed for the additives used in this study was BBr_3 > TMA > N_2H_4 > $TiCl_4$ as indicated by the residual hydrogen wt % upon complete dehydrogenation at 500 °C. TMA exhibits the most promising results with release of H_2 as low as 90 °C and the majority of H_2 content released in a step 100 °C lower than observed for unmodified $Mg(BH_4)_2$. The N_2H_4-exposed sample also yielded unexpected results by generating surface-limited ammonia borane and/or hydrazine borane/bis-borane on γ-$Mg(BH_4)_2$, with both pathways possible depending on the extent of N_2H_4 hydration. Our hope is that this unconventional approach can lead to a new class of mixed hydridic-protonic composite materials.

■ ASSOCIATED CONTENT

Supporting Information

The Supporting Information is available free of charge at https://pubs.acs.org/doi/10.1021/acsaem.1c03128.

Raman spectra; TPD data; ^{11}B {^1H} SS NMR spectra of the additive–$Mg(BH_4)_2$ mixtures not shown in the main text; and ^{27}Al MAS SS NMR spectrum of γ-$Mg(BH_4)_2$ exposed to 100 pulses of TMA (PDF)

■ AUTHOR INFORMATION

Corresponding Author

Steven T. Christensen − *National Renewable Energy Laboratory, Golden, Colorado 80401, United States*; Email: Steven.Christensen@NREL.gov

Authors

Nicholas A. Strange − *National Renewable Energy Laboratory, Golden, Colorado 80401, United States; SLAC National Accelerator Laboratory, Menlo Park, California 94025, United States*; orcid.org/0000-0001-5699-7274

Noemi Leick − *National Renewable Energy Laboratory, Golden, Colorado 80401, United States*; orcid.org/0000-0002-2014-6264

Sarah Shulda − *National Renewable Energy Laboratory, Golden, Colorado 80401, United States*

Andreas Schneemann − *Sandia National Laboratories, Livermore, California 94550, United States*

Vitalie Stavila − *Sandia National Laboratories, Livermore, California 94550, United States*; orcid.org/0000-0003-0981-0432

Andrew S. Lipton − *Pacific Northwest National Laboratory, Richland, Washington 99354, United States*; orcid.org/0000-0003-4937-4145

Michael F. Toney − *SLAC National Accelerator Laboratory, Menlo Park, California 94025, United States; Department of Chemical and Biological Engineering and Renewable and Sustainable Energy Institute (RASEI), University of Colorado Boulder, Boulder, Colorado 80309, United States*; orcid.org/0000-0002-7513-1166

Thomas Gennett − *National Renewable Energy Laboratory, Golden, Colorado 80401, United States; Chemistry Department, Colorado School of Mines, Golden, Colorado 80401, United States*

Complete contact information is available at: https://pubs.acs.org/10.1021/acsaem.1c03128

Notes

The authors declare no competing financial interest.

■ ACKNOWLEDGMENTS

This work was supported by the U.S. Department of Energy under contract no. DE-AC36-08GO28308 with the Alliance for Sustainable Energy, LLC, the manager and operator of the National Renewable Energy Laboratory (NREL) (N.A.S., N.L., S.S., T.G., and S.C.). Sandia National Laboratories is a

multimission laboratory managed and operated by National Technology and Engineering Solutions of Sandia, LLC., a wholly owned subsidiary of Honeywell International, Inc., for the U.S. Department of Energy's National Nuclear Security Administration (NNSA) under contract DE-NA-0003525 (A.S., V.S.). Use of the Stanford Synchrotron Radiation Lightsource, SLAC National Accelerator Laboratory, is supported by the U.S. Department of Energy, Office of Science, Office of Basic Energy Sciences under contract no. DE-AC02-76SF00515. The authors thank Kevin Stone, Chris Tassone, Tim Dunn, and J.R. Troxel for their skillful assistance in advance of and during measurements performed at SSRL. A portion of the research was performed using EMSL (grid.436923.9), a DOE Office of Science User Facility sponsored by the Office of Biological and Environmental Research. The authors (N.A.S., N.L., S.S., A.S., V.S., and S.C.) gratefully acknowledge research support from the Hydrogen Materials—Advanced Research Consortium (HyMARC), established as part of the Energy Materials Network under the U.S. Department of Energy, Office of Energy Efficiency and Renewable Energy, Hydrogen Fuel Cell Technologies Office, under contract DE-AC36-08GO28308. The views expressed in the article do not necessarily represent the views of the DOE or the U.S. Government.

REFERENCES

(1) Ministerial Council on Renewable Energy. Hydrogen and Related Issues, Basic Hydrogen Strategy. https://www.meti.go.jp/english/press/2017/1226_003.html (accessed 2021-05-21).

(2) Study Task Force. Hydrogen Roadmap Korea. https://www.iea.org/policies/6566-korea-hydrogen-economy-roadmap-2040 (accessed 2021-05-21).

(3) Federal Ministry for Economic Affairs and Energy Public Relations Division. The National Hydrogen Strategy. https://www.bmbf.de/files/bmwi_Nationale%20Wasserstoffstrategie_Eng_s01.pdf (accessed 2021-05-21).

(4) United States Department of Energy. Hydrogen Program Plan. https://www.hydrogen.energy.gov/pdfs/hydrogen-program-plan-2020.pdf, (accessed 2021-05-21

(5) Kollonitsch, J.; Fuchs, O.; Gabor, V. Alkaline-Earth Borohydrides and Their Applications in Organic Syntheses. *Nature* **1955**, *175*, 346.

(6) Heere, M.; Hansen, A.-L.; Payandeh, S.; Aslan, N.; Gizer, G.; Sørby, M. H.; Hauback, B. C.; Pistidda, C.; Dornheim, M.; Lohstroh, W. Dynamics of Porous and Amorphous Magnesium Borohydride to Understand Solid State Mg-Ion-Conductors. *Sci. Rep.* **2020**, *10*, 9080.

(7) Møller, K.; Sheppard, D.; Ravnsbæk, D.; Buckley, C.; Akiba, E.; Li, H.-W.; Jensen, T.; Id, K. T. M.; Sheppard, D.; Ravnsbæk, D. B.; Akiba, E.; Li, H. W.; Jensen, T. R. Complex Metal Hydrides for Hydrogen, Thermal and Electrochemical Energy Storage. *Energies* **2017**, *10*, 1645.

(8) US Department of Energy. DOE Technical Targets for Onboard Hydrogen Storage for Light-Duty Vehicles. https://www.energy.gov/eere/fuelcells/doe-technical-targets-onboard-hydrogen-storage-light-duty-vehicles (accessed 2021-05-21).

(9) Filinchuk, Y.; Richter, B.; Jensen, T. R.; Dmitriev, V.; Chernyshov, D.; Hagemann, H. Porous and Dense Magnesium Borohydride Frameworks: Synthesis, Stability, and Reversible Absorption of Guest Species. *Angew. Chem., Int. Ed.* **2011**, *123*, 11358−11362.

(10) Zavorotynska, O.; Deledda, S.; Li, G.; Matsuo, M.; Orimo, S.-i.; Hauback, B. C. Isotopic Exchange in Porous and Dense Magnesium Borohydride. *Angew. Chem., Int. Ed.* **2015**, *54*, 10592−10595.

(11) David, W. I. F.; Callear, S. K.; Jones, M. O.; Aeberhard, P. C.; Culligan, S. D.; Pohl, A. H.; Johnson, S. R.; Ryan, K. R.; Parker, J. E.; Edwards, P. P.; Nuttall, C. J.; Amieiro-Fonseca, A. The Structure, Thermal Properties and Phase Transformations of the Cubic Polymorph of Magnesium Tetrahydroborate. *Phys. Chem. Chem. Phys.* **2012**, *14*, 11800−11807.

(12) Paskevicius, M.; Pitt, M. P.; Webb, C. J.; Sheppard, D. A.; Filsø, U.; Gray, E. M.; Buckley, C. E. In-Situ X-ray Diffraction Study of γ-Mg(BH4)2 Decomposition. *J. Phys. Chem. C* **2012**, *116*, 15231−15240.

(13) Chong, M.; Autrey, T.; Jensen, C. Lewis Base Complexes of Magnesium Borohydride: Enhanced Kinetics and Product Selectivity upon Hydrogen Release. *Inorganics* **2017**, *5*, 89.

(14) Newhouse, R. J.; Stavila, V.; Hwang, S.-J.; Klebanoff, L. E.; Zhang, J. Z. Reversibility and Improved Hydrogen Release of Magnesium Borohydride. *J. Phys. Chem. C* **2010**, *114*, 5224−5232.

(15) Zhang, Z. G.; Wang, H.; Liu, J. W.; Zhu, M. Thermal Decomposition Behaviors of Magnesium Borohydride Doped with Metal Fluoride Additives. *Thermochim. Acta* **2013**, *560*, 82−88.

(16) Amieiro-Fonseca, A.; Ellis, S. R.; Nuttall, C. J.; Hayden, B. E.; Guerin, S.; Purdy, G.; Soulié, J.-P.; Callear, S. K.; Culligan, S. D.; David, W. I. F.; Edwards, P. P.; Jones, M. O.; Johnson, S. R.; Pohl, A. H. A Multidisciplinary Combinatorial Approach for Tuning Promising Hydrogen Storage Materials towards Automotive Applications. *Faraday Discuss.* **2011**, *151*, 369−384.

(17) Matsumura, D.; Ohyama, T.; Okajima, Y.; Nishihata, Y.; Li, H.-W.; Orimo, S.-i. Correlation between Structure of Titanium Additives and Dehydrogenation Reaction of Magnesium Borohydride Studied by Continuous Observation of X-Ray Absorption Spectroscopy. *Mater. Trans.* **2011**, *52*, 635−640.

(18) Li, H.-W.; Kikuchi, K.; Nakamori, Y.; Miwa, K.; Towata, S.; Orimo, S. Effects of ball milling and additives on dehydriding behaviors of well-crystallized Mg(BH4)2. *Scr. Mater.* **2007**, *57*, 679−682.

(19) Heere, M.; Zavorotynska, O.; Deledda, S.; Sørby, M. H.; Book, D.; Steriotis, T.; Hauback, B. C. Effect of Additives, Ball Milling and Isotopic Exchange in Porous Magnesium Borohydride. *RSC Adv.* **2018**, *8*, 27645−27653.

(20) Zanella, P.; Crociani, L.; Masciocchi, N.; Giunchi, G. Facile High-Yield Synthesis of Pure, Crystalline Mg(BH4)2. *Inorg. Chem.* **2007**, *46*, 9039−9041.

(21) Hoffman, A. S.; Singh, J. A.; Bent, S. F.; Bare, S. R. In Situ Observation of Phase Changes of a Silica-Supported Cobalt Catalyst for the Fischer-Tropsch Process by the Development of a Synchrotron-Compatible in Situ/Operando Powder X-Ray Diffraction Cell. *J. Synchrotron Radiat.* **2018**, *25*, 1673−1682.

(22) Walter, E. D.; Qi, L.; Chamas, A.; Mehta, H. S.; Sears, J. A.; Scott, S. L.; Hoyt, D. W. Operando MAS NMR Reaction Studies at High Temperatures and Pressures. *J. Phys. Chem. C* **2018**, *122*, 8209−8215.

(23) Hahn, E. L. Spin Echoes. *Phys. Rev.* **1950**, *80*, 580−594.

(24) Sinha, N.; Grant, C. V.; Wu, C. H.; De Angelis, A. A.; Howell, S. C.; Opella, S. J. SPINAL Modulated Decoupling in High Field Double- and Triple-Resonance Solid-State NMR Experiments on Stationary Samples. *J. Magn. Reson.* **2005**, *177*, 197−202.

(25) Hurst, K. E.; Heben, M. J.; Blackburn, J. L.; Gennett, T.; Dillon, A. C.; Parilla, P. A. A Dynamic Calibration Technique for Temperature Programmed Desorption Spectroscopy. *Rev. Sci. Instrum.* **2013**, *84*, 025103.

(26) Hirao, H.; Omoto, K.; Fujimoto, H. Lewis Acidity of Boron Trihalides. *J. Phys. Chem. A* **1999**, *103*, 5807−5811.

(27) Ferrari, A.; Giorgio, F. La Struttura Cristallina Dei Bromuri Di Metalli Bivalenti. *Atti della Accad. Naz. dei Lincei, Cl. di Sci. Fis. Mat. e Nat. Rend.* **1929**, *9*, 1134−1140.

(28) Dimitrievska, M.; White, J. L.; Zhou, W.; Stavila, V.; Klebanoff, L. E.; Udovic, T. J. Structure-dependent vibrational dynamics of Mg(BH4)2 polymorphs probed with neutron vibrational spectroscopy and first-principles calculations. *Phys. Chem. Chem. Phys.* **2016**, *18*, 25546−25552.

(29) Hagemann, H.; D'Anna, V.; Rapin, J.-P.; Černý, R.; Filinchuk, Y.; Kim, K. C.; Sholl, D. S.; Parker, S. F. New fundamental

https://doi.org/10.1021/acsaem.1c03128
ACS Appl. Energy Mater. 2022, 5, 1690−1700

experimental studies on α-Mg(BH4)2 and other borohydrides. *J. Alloys Compd.* **2011**, *509*, S688−S690.
(30) Giannasi, A.; Colognesi, D.; Ulivi, L.; Zoppi, M.; Ramirez-Cuesta, A. J.; Bardají, E. G.; Roehm, E.; Fichtner, M. High Resolution Raman and Neutron Investigation of Mg(BH4)2 in an Extensive Temperature Range. *J. Phys. Chem. A* **2010**, *114*, 2788−2793.
(31) Lauermannova, A.-M.; Lojka, M.; Antoncik, F.; Sedmidubsky, D.; Pavlikova, M.; Pavlik, Z.; Janovsky, O. Graphene- and Graphite Oxide-reinforced Magnesium Oxychloride Cement Composites for the Construction Use. *Appl. Sci.* **2020**, *10*, 1−9.
(32) Weir, C. E.; Schroeder, R. A. Infrared Spectra of the Crystalline Inorganic Borates. *J. Res. Natl. Bur. Stand. A. Phys. Chem.* **1964**, *68*, 465−487.
(33) Jeong, S.; Heo, T. W.; Oktawiec, J.; Shi, R.; Kang, S.; White, J. L.; Schneemann, A.; Zaia, E. W.; Wan, L. F.; Ray, K. G.; Liu, Y.-S.; Stavila, V.; Guo, J.; Long, J. R.; Wood, B. C.; Urban, J. J. A Mechanistic Analysis of Phase Evolution and Hydrogen Storage Behavior in Nanocrystalline Mg(BH4)2 within Reduced Graphene Oxide. *ACS Nano* **2020**, *14*, 1745−1756.
(34) Leick, N.; Strange, N. A.; Schneemann, A.; Stavila, V.; Gross, K.; Washton, N.; Settle, A.; Martinez, M. B.; Gennett, T.; Christensen, S. T. Al2O3 Atomic Layer Deposition on Nanostructured γ-Mg(BH4)2 for H2 Storage. *ACS Appl. Energy Mater.* **2021**, *4*, 1150−1162.
(35) Sethio, D.; Lawson Daku, L. M.; Hagemann, H. A theoretical study of the spectroscopic properties of B2H6 and of a series of BHyz− species (x = 1−12, y = 3−14, z = 0−2): From BH3 to B12H122−. *Int. J. Hydrogen Energy* **2016**, *41*, 6814−6824.
(36) Cotton, F. A.; Wilkinson, G. *Advanced Inorganic Chemistry*; John Wiley and Sons, Inc., 1972.
(37) Brown, H. C.; Ravindran, N.; Brown, H. C.; Ravindran, N. Molecular addition compounds. 3. Redistribution of borane-methyl sulfide with boron trichloride-methyl sulfide and boron tribromide-methyl sulfide as convenient routes to the corresponding haloborane-methyl sulfides. *J. Am. Chem. Soc.* **1977**, *16*, 2938−2940.
(38) Kroeker, S.; Stebbins, J. F. Three-Coordinated Boron-11 Chemical Shifts in Borates. *Inorg. Chem.* **2001**, *40*, 6239−6246.
(39) Beckett, P.; Denning, M. S.; Heinmaa, I.; Dimri, M. C.; Young, E. A.; Stern, R.; Carravetta, M. High resolution 11B NMR of magnesium diboride using cryogenic magic angle spinning. *J. Chem. Phys.* **2012**, *137*, 114201.
(40) Setijadi, E. J.; Boyer, C.; Aguey-Zinsou, K.-F. Remarkable hydrogen storage properties for nanocrystalline MgH2 synthesised by the hydrogenolysis of Grignard reagents. *Phys. Chem. Chem. Phys.* **2012**, *14*, 11386−11397.
(41) Davis-Gilbert, Z. W.; Tonks, I. A. Titanium Redox Catalysis: Insights and Applications of an Earth-Abundant Base Metal. *Dalton Trans.* **2017**, *46*, 11522−11528.
(42) Shi, E.; Wang, A.; Ling, Z.; VNIR, N. I. R. MIR, VNIR, NIR, and Raman spectra of magnesium chlorides with six hydration degrees: Implication for Mars and Europa. *J. Raman Spectrosc.* **2020**, *51*, 1589−1602.
(43) Hino, S.; Fonneløp, J. E.; Corno, M.; Zavorotynska, O.; Damin, A.; Richter, B.; Baricco, M.; Jensen, T. R.; Sørby, M. H.; Hauback, B. C. Halide Substitution in Magnesium Borohydride. *J. Phys. Chem. C* **2012**, *116*, 12482−12488.
(44) Hoekstra, H. R.; Katz, J. J. The Preparation and Properties of the Group IV-B Metal Borohydrides. *J. Am. Chem. Soc.* **1949**, *71*, 2488−2492.
(45) Fitzgerald, M.; Leick, N.; Gross, K.; Christensen, S.; Pylypenko, S. Multi-Technique Characterization of Atomic-Layer-Deposition-Functionalized Magnesium Borohydride Hydrogen Storage Materials. *APS March Meeting*, 2020;.
(46) He, T.; Wu, H.; Chen, J.; Zhou, W.; Wu, G.; Xiong, Z.; Zhang, T.; Chen, P. Alkali and Alkaline-Earth Metal Borohydride Hydrazinates: Synthesis, Structures and Dehydrogenation. *Phys. Chem. Chem. Phys.* **2013**, *15*, 10487−10493.
(47) Gervais, C.; Framery, E.; Duriez, C.; Maquet, J.; Vaultier, M.; Babonneau, F. 11B and 15N solid state NMR investigation of a boron nitride preceramic polymer prepared by ammonolysis of borazine. *J. Eur. Ceram. Soc.* **2005**, *25*, 129−135.
(48) Heldebrant, D. J.; Karkamkar, A.; Linehan, J. C.; Autrey, T. Synthesis of Ammonia Borane for Hydrogen Storage Applications. *Energy Environ. Sci.* **2008**, *1*, 156−160.
(49) Moury, R.; Demirci, U. Hydrazine Borane and Hydrazinidoboranes as Chemical Hydrogen Storage Materials. *Energies* **2015**, *8*, 3118−3141.
(50) Moury, R.; Moussa, G.; Demirci, U. B.; Hannauer, J.; Bernard, S.; Petit, E.; Van Der Lee, A.; Miele, P.; Der Lee, V.; Miele, P. Hydrazine Borane: Synthesis, Characterization, and Application Prospects in Chemical Hydrogen Storage. *Phys. Chem. Chem. Phys.* **2012**, *14*, 1768−1777.
(51) Hügle, T.; Kühnel, M. F.; Lentz, D. Hydrazine Borane: A Promising Hydrogen Storage Material. *J. Am. Chem. Soc.* **2009**, *131*, 7444−7446.
(52) Chua, Y. S.; Pei, Q.; Ju, X.; Zhou, W.; Udovic, T. J.; Wu, G.; Xiong, Z.; Chen, P.; Wu, H. Alkali Metal Hydride Modification on Hydrazine Borane for Improved Dehydrogenation. *J. Phys. Chem. C* **2014**, *118*, 11244−11251.
(53) Finnie, K. S.; Cassidy, D. J.; Bartlett, J. R.; Woolfrey, J. L. IR Spectroscopy of Surface Water and Hydroxyl Species on Nanocrystalline TiO2 Films. *Langmuir* **2001**, *17*, 816−820.
(54) Pylypko, S.; Petit, E.; Yot, P. G.; Salles, F.; Cretin, M.; Miele, P.; Demirci, U. B. Key Study on the Potential of Hydrazine Bisborane for Solid- and Liquid-State Chemical Hydrogen Storage. *Inorg. Chem.* **2015**, *54*, 4574−4583.
(55) Fichtner, M.; Zhao-Karger, Z.; Hu, J.; Roth, A.; Weidler, P. The kinetic properties of Mg(BH4)2infiltrated in activated carbon. *Nanotechnology* **2009**, *20*, 204029.
(56) Yang, J.; Fu, H.; Song, P.; Zheng, J.; Li, X. Reversible dehydrogenation of Mg(BH4)2-LiH composite under moderate conditions. *Int. J. Hydrogen Energy* **2012**, *37*, 6776−6783.
(57) Kalantzopoulos, G. N.; Vitillo, J. G.; Albanese, E.; Pinatel, E.; Civalleri, B.; Deledda, S.; Bordiga, S.; Baricco, M.; Hauback, B. C. Hydrogen Storage of Mg-Zn Mixed Metal Borohydrides. *J. Alloys Compd.* **2014**, *615*, S702−S705.

https://doi.org/10.1021/acsaem.1c03128
ACS Appl. Energy Mater. 2022, 5, 1690−1700